Journal of Sol-Gel Science and Technology (2019) 89:754–763
https://doi.org/10.1007/s10971-018-4871-z

ORIGINAL PAPER: SOL-GEL AND HYBRID MATERIALS FOR ENERGY, ENVIRONMENT AND BUILDING APPLICATIONS

Synthesis of silver decorated silica nanoparticles with rough surfaces as adsorbent and catalyst for methylene blue removal

Mengqing Hu[1] · Xinlong Yan[1] · Xiaoyan Hu[1] · Rui Feng[1] · Min Zhou[1]

Received: 3 September 2018 / Accepted: 29 October 2018 / Published online: 9 November 2018

Abstract

The discharge of dyes from industries to water reservoirs has attracted extensive attention worldwide, and it is of great importance to remove them efficiently. In this study, a series of silica nanoparticles with rough surfaces was prepared, and highly dispersed silver nanoparticles were loaded on its surface through a simple wet-impregnation method. The adsorption performance and catalytic activity of the as-prepared Ag/SiO_2 for methylene blue (MB) removal was investigated. The results demonstrated that the Ag/SiO_2 with smaller particle size and higher Ag loading amount shows high adsorption capacity and catalytic activity for MB. The maximum adsorption capacity was found to be ~55 mg/g, which is more than two times of pure silica nanoparticles. Besides, MB could be degraded by more than 99% of the initial concertation (40 mg/L) within 3 min and rate constant of the catalytic reduction achieved as high as 2.128 min^{-1}. Moreover, the as-prepared Ag/SiO_2 shows good stability in acidic environment and excellent reusability for at least eight successive cycles of adsorption and four cycles of catalytic reduction.

Graphical Abstract

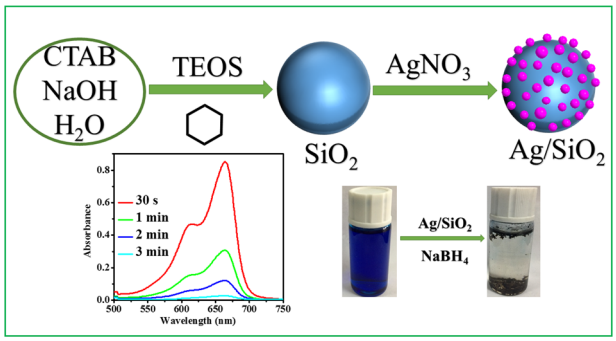

Highlights

- Highly dispersed Ag nanoparticles on rough surface of silica spheres were prepared.
- Ag decorated silica shows good adsorption and catalytic capability for MB removal.
- MB could be catalytically degraded to < 1% of the initial concentration within 3 min.

Electronic supplementary material The online version of this article (https://doi.org/10.1007/s10971-018-4871-z) contains supplementary material, which is available to authorized users.

✉ Xinlong Yan
yanxl@cumt.edu.cn

[1] Key Laboratory of Coal Processing and Efficient Utilization (Ministry of Education), School of Chemical Engineering & Technology, China University of Mining and Technology, XuZhou 221116, PR China

Keywords Silver decorated SiO_2 · Catalyst · Adsorption · Reduction · Methylene blue

1 Introduction

Water pollution caused by organic contaminants has posed a great threat to human life and health. Among many organic pollutants, organic dyes are receiving extensive attention because large numbers of industrial produced wastewater containing organic dyes were discharged into water body directly [1, 2]. Therefore, it is imperative to seek some ways to remove organic dye from water.

At present, various technologies have been exploited to remove organic dyes from water, such as adsorption [3, 4], catalytic oxidation [5–7], photocatalytic degradation [8, 9], membrane filtration [10], electrochemical method [11], and biological method [12]. Among them, adsorption and catalytic degradation are considered as the most effective and reliable technique for treatment of wastewater, due to its high efficiency, easy operation and relatively low cost etc. [13, 14]. Therefore, various adsorbents and catalysts are designed and developed to remove dyes from water, such as porous carbon [15], metal oxides [16], graphene oxide [17], Mg-Al layered double hydroxide [18], and mesoporous silica [19].

Recently, reduction of dyes into biodegradable pollutants in the presence of $NaBH_4$ was developed as a new and efficient technique for wastewater treatment [20–22]. And silver nanoparticles were found to be a good catalyst with excellent performance [23–25]. However, direct use of silver nanoparticle often suffer from their susceptibility to coagulation and agglomeration, moreover, silver is a precious metal and reducing the amount of silver used is one of the most effective ways to cut the cost. To overcome these shortbacks, immobilization of silver onto different support materials was developed as novel adsorbent or catalyst to remove organic dyes from water. Zhu et al. synthesized [26] silver-doped mesoporous silica fiber for methylene blue reduction; Lee et al. reported [27] the fabrication of silver nanoparticles decorated graphene–carbon sphere hybrid aerogel for adsorption of MB from water. Nasrollahzadeh et al. used [28, 29] seashell and perlite as the support for silver nanoparticles and investigated their catalytic activity for reduction of organic dyes. However, most of the reported composites are limited by relatively long degradation time or poor cyclic stability, which makes it challenging to recycle and reuse the adsorbents efficiently, further affecting their decontamination efficiencies in dye removal.

In this work, a series of silica spheres with rough surface were synthesized by controlling the formation time of silica. Then, silver nanoparticles were loaded onto the surface of silica sphere through a wet-impregnation method. The above obtained Ag/SiO_2 composites were further used as adsorbent for MB removal from water, besides, its catalytic activity was studied by monitoring the reduction of MB by an excess of $NaBH_4$. The results showed that the Ag/SiO_2 composite exhibited good catalytic and adsorption properties for MB removal. In addition, it maintains good catalytic performance in a wide range of solution pH and exhibits good recycle stability.

2 Experimental details

2.1 Materials

All reagents used were of analytical grade and were purchased from Sinoreagent Company (Shanghai, China), including hexadecyltrimethylammonium bromide (CTAB), tetraethoxysilane (TEOS), cyclohexane, silver nitrate ($AgNO_3$), sodium borohydride ($NaBH_4$), NaOH, aqueous ammonia, ethanol, and Methylene blue (MB).

2.2 Synthesis of silica nanoparticles with rough surfaces

A series of silica nanoparticles with rough surfaces were synthesized according to Zhao et al. [30]. Typically, 1.0 g of CTAB and 0.8 mL of NaOH (0.1 M) were added into 50 mL of deionized water under stirring, and the solution was continuously stirred at 60 °C for 2 h. Then 20 mL of TEOS and 1 mL of cyclohexane mixture solution was added to the above solution and kept at 60 °C with stirring for 6, 12, 24, and 48 h, respectively. After that, the products were collected by centrifuging and washed by ethanol for three times. Then, the samples were dispersed in 50 mL of ethanol and refluxed at 70 °C for 12 h to remove CTAB. Finally, the products were washed with ethanol and dried in vacuum at 45 °C for 12 h. The as-prepared samples were marked as SiO_2-6, SiO_2-12, SiO_2-24, and SiO_2-48, respectively.

2.3 Synthesis of Ag/SiO_2 composites

The Ag decorated SiO_2 nanoparticles were synthesized by using wet-impregnation method. Typically, 100 mg of as-prepared SiO_2-6, SiO_2-12, SiO_2-24, or SiO_2-48 were dispersed in a mixed solution of 100 mL ethanol and 5 mL ammonia under stirring for 5 min, respectively, and then the solution was ultrasonication for 10 min. Afterwards, a

solution of 0.4 g of $AgNO_3$ dispersed in 20 mL ethanol was rapidly poured into the above mixture under continuous ultrasonication for 40 min. Finally, the obtained Ag/SiO_2 was washed three times with water and ethanol. The products were collected by centrifugation, and dried in vacuum for 12 h at 90 °C. The obtained samples were marked as Ag/SiO_2-6, Ag/SiO_2-12, Ag/SiO_2-24, and Ag/SiO_2-48, respectively.

2.4 Characterization

Powder X-ray diffraction patterns (XRD) were recorded by a Bruker D8 ADVANCE diffractomer with Cu K-α radiation (40 KV, 30 mA). The morphology of the samples was examined using scanning electron microscope (SEM) (FEI Quanta 400 FEG) and transmission electron microscope (TEM) (FEI Tecnai G2 F20). N_2 adsorption–desorption experiments were performed in a Quantachrome iQ2 porosimeter after degassing the samples at 100 °C for 12 h. The Brunauer–Emmet–Teller (BET) method was used to calculate the specific surface area. Content of silver in the composite materials were analyzed by using inductively coupled plasma optical emission spectrometry (ICP-MS, Agilent 7900). X-ray photoelectron spectrum (XPS) measurements were performed on a Thermo Scientific Escalab 250Xi instrument equipped with Al Kα radiation. Thermogravimetric analysis (TGA, Netzsch STA 449 F5) was performed under Ar gas at a flow rate of 100 cm^3/min. The sample was heated from 30 to 800 °C with a temperature ramp rate of 10 °C/min. FT-IR spectra were collected by a Thermo Nicolet iS5 spectrometer in transmission mode over the range of 4000–400 cm^{-1}. The zeta potential of the sample at different solution pH was determined by a Brookhaven Zeta-PALS instrument.

2.5 Adsorption experiment

The MB adsorption isotherms were acquired by the adsorption measurements performed with 5 mg of solid samples dispersed in a series of 25 mL of solutions with different MB concentrations (10 mg/L-50 mg/L) under stirring for 12 h at 25 °C. At the end of adsorption, the solution was collected by filtration, and the concentration of MB was measured with an UV–Vis spectrophotometer (TU-1810, Persee Co., China). The capacity of MB adsorbed onto the samples was calculated using the following equation:

$$q_e = \frac{(C_0 - C_e)V}{M}$$

where q_e is the capacity of MB adsorbed at equilibrium; C_0 and C_e are the initial and equilibrium concentration of MB, respectively; V is the volume (L) of solution; and M is the sample weight used.

2.6 Catalytic reduction of MB

Catalytic reduction of MB was conducted in a beaker containing 10 mg of sample dispersed in 20 mL of MB aqueous solution (40 mg/L) with 1 mL of fresh $NaBH_4$ aqueous solution (0.1 mol/L) injected under stirring. The concentration of MB in solution was monitored by measuring the absorbance values at 665 nm using a UV–Vis spectrophotometer.

The catalytic degradation fraction of the dyes can be expressed in the following equation:

$$\text{Dye removal } (\%) = \frac{A_0 - A_t}{A_0}$$

where A_0 is the absorbance of MB solution before reaction and A_t is the absorbance of MB at time t of the catalytic reaction. The reaction rate constant k_{app} was calculated using the pseudo-first-order kinetics equation:

$$\ln\frac{A_t}{A_0} = -k_{app}t$$

3 Results and discussion

3.1 Characterization of materials

Figure 1 shows the XRD patterns of Ag/SiO_2 composites. A wide diffraction peak at ~22.8° (2θ) corresponding to the amorphous SiO_2 could be observed for all samples [31]. Moreover, four diffraction peaks located at $2\theta = 38.36°$, 44.32°, 64.58°, and 77.51° can be ascribed to (111), (200), (220), and (311) planes of silver crystals, respectively,

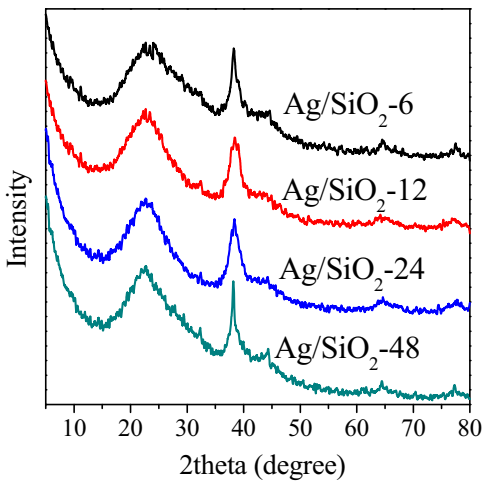

Fig. 1 XRD patterns of Ag/SiO_2 samples

indicating the existence of silver crystals with face centered cubic structure in the composites [32, 33]. The Ag content in Ag/SiO_2 composites analyzed by ICP were 3.5 wt%, 4.9 wt%, 6.7 wt%, and 6.0 wt% for Ag/SiO_2-6, Ag/SiO_2-12, Ag/SiO_2-24, and Ag/SiO_2-48 samples, respectively (Table 1).

The morphology of different SiO_2 and Ag modified SiO_2 was characterized by TEM and SEM. For pure SiO_2, particles with rough surfaces could be seen for all samples (Fig. S1). With increasing hydrothermal time from 6 to 48 h during the synthesis, the diameter of SiO_2 particles increased. However, the particle size barely changed with further increase of hydrothermal time. For Ag decorated silica (Fig. 2), the morphology was not much different from their parent silica, except the appearance of small black dots, which could be convinced that these dots are silver particles. With the increase of hydrothermal time of silica from 6 to 48 h, the content of silver in the Ag/silica composite slightly increased, and the particle size increased from ~25 to ~101 nm, while the size of silver particle in all Ag/silica were found to be ~10 to ~13 nm. According to the high-resolution TEM picture and energy-dispersive X-ray spectroscopy (EDX) results (Fig. 2e, f), detectable Ag in Ag/SiO_2-48 sample further confirmed that silver was loaded onto silica successfully. (Note that Cu peaks came from the TEM grid.) Furthermore, SEM (Fig. 3a–d) images show that all samples have similar sphere-like shapes with rough surfaces. Among these samples, Ag/SiO_2-24 was selected for further analysis by using EDX elemental mapping (Fig. 3e–h). The result shown in Fig. 3h reveals that silver atoms are homogenously dispersed on the surface of SiO_2 matrix.

Table 1 Surface area, porosity data and Ag content of Ag/SiO_2 samples

Samples	S_{BET} (m^2/g)	V_t (cm^3/g)	W_{Ag}/W_{sample} (wt%)
Ag/SiO_2-6	216	0.80	3.5
Ag/SiO_2-12	210	0.77	4.9
Ag/SiO_2-24	208	0.76	6.7
Ag/SiO_2-48	199	0.66	6.0
SiO_2-6	292	1.09	0
SiO_2-12	218	0.81	0
SiO_2-24	262	0.91	0
SiO_2-48	261	0.76	0

Figure 4a and S2a displayed N_2 adsorption–desorption isotherms of Ag/SiO_2 and SiO_2 samples. Clearly, all Ag/SiO_2 and SiO_2 samples exhibited type IV isotherm, which is characteristic of mesoporous material [34, 35]. There is a decrease of surface area and pore volume for all composites after silver impregnation as revealed in Table 1. The pore size distributions of different Ag/SiO_2 and SiO_2 materials were analyzed by NLDFT method. All the Ag/SiO_2 samples showed similar pore size distributions compared with their parent silica (Fig. S2b and Fig. 4b). It can also be seen that pore size of the Ag/SiO_2 composites decreased slightly with increased formation time of silica. The pore size distribution of Ag/SiO_2-6 sample is much different with other Ag/SiO_2 samples. It has mesopores with a size centered at around 43 nm. The relatively large pore size may cause the easy pour of the Ag precursor, thus, the Ag content in the resulting samples are relatively low.

To further investigate the valence state of different species on SiO_2 samples, XPS analysis was conducted and the results are shown in Fig. 5. All of the peaks on the survey spectrum of Ag/SiO_2-24 composite can be assigned to Ag, O, and Si elements, which is well consistent with the EDX analysis. Two peaks at ~368 eV and ~374 eV in the high-resolution XPS spectrum of Ag 3d region can be assigned to

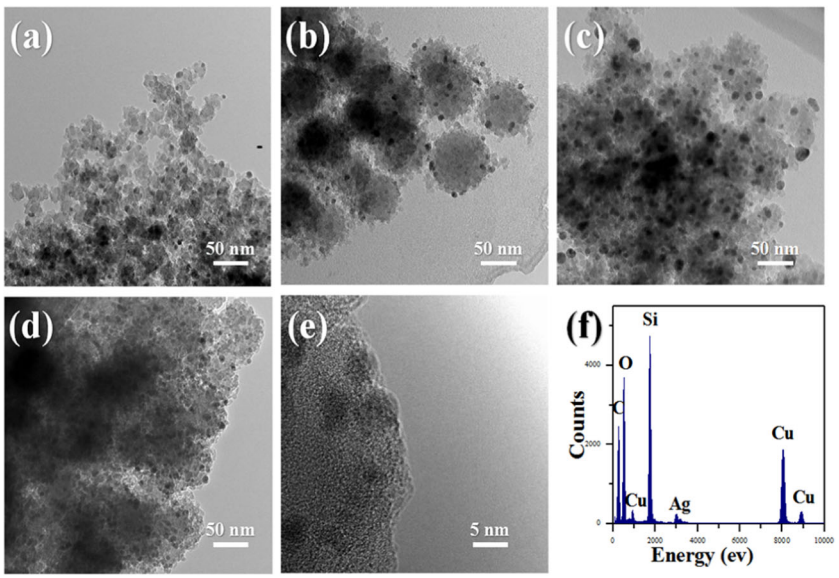

Fig. 2 TEM images of **a** Ag/SiO_2-6, **b** Ag/SiO_2-12, **c** Ag/SiO_2-24, **d–e** Ag/SiO_2-48, and **f** EDX analysis of the Ag/SiO_2-48

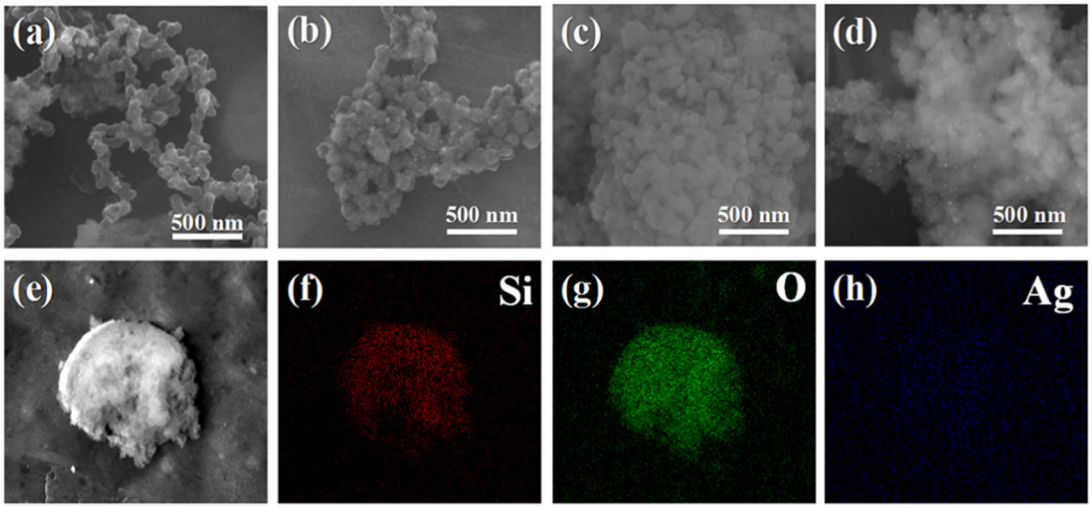

Fig. 3 SEM images of **a** Ag/SiO_2-6, **b** Ag/SiO_2-12, **c** Ag/SiO_2-24, **d** Ag/SiO_2-48, and **e–h** elemental mapping images (9223× magnification) of the Ag/SiO_2-24

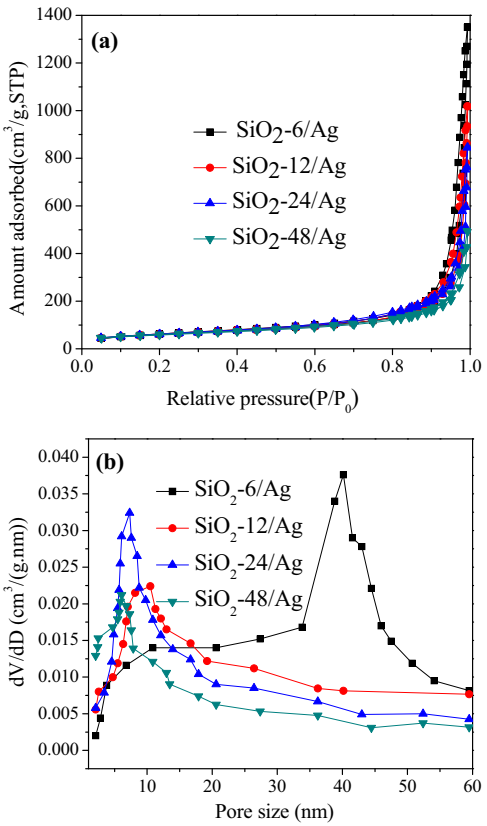

Fig. 4 **a** Nitrogen adsorption–desorption isotherms and **b** pore size distributions of Ag/SiO_2 samples (NLDFT method)

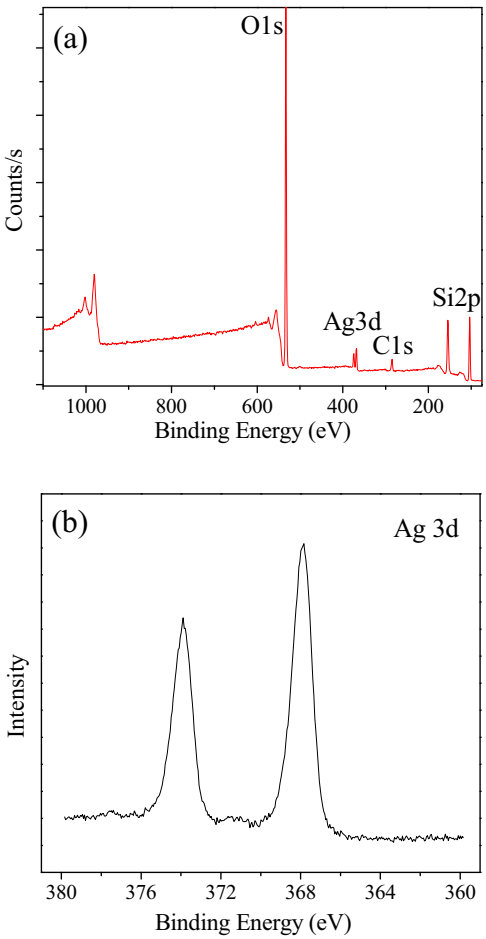

Fig. 5 XPS survey **a** and high-resolution Ag 3d spectra **b** of Ag/SiO_2-24 sample

Ag $3d_{5/2}$ and Ag $3d_{3/2}$, indicating the formation of metallic Ag^0 at surface of Ag/SiO_2-24 sample [24].

TG curves of SiO_2 and Ag/SiO_2-24 samples were shown in Fig. S3, little weight change caused by desorption of moisture can be seen for both samples, which indicates the high thermal stability of the samples.

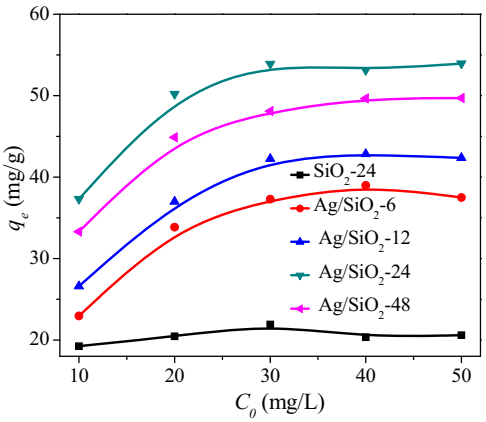

Fig. 6 Adsorption isotherms of MB onto different samples. (MB concentration = 10–50 mg/L, solution volume = 25 mL, Ag/SiO_2 = 5 mg, T = 25 °C)

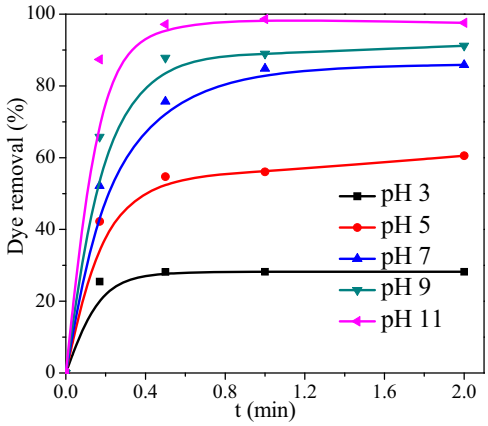

Fig. 7 Fraction of degraded dye for adsorption of MB by Ag/SiO_2-24 sample under various pH conditions. (MB = 10 mg/L, solution volume = 20 mL, Ag/SiO_2-24 = 10 mg, T = 25 °C)

Table 2 Comparison of adsorption capacity for MB with different silver composites

samples	MB volume (mL)	adsorbent (g/L)	Ag content (g/L)	adsorption capacity (mg/g)
Ag/SiO_2-6	25	0.2	0.007	37
Ag/SiO_2-12	25	0.2	0.0098	42
Ag/SiO_2-24	25	0.2	0.013	55
Ag/SiO_2-48	25	0.2	0.012	49
SiO_2-24	25	0.2	0	20

3.2 Adsorption of MB

The adsorption capacities of the as-synthesized composites at different MB concentration were tested and the results are shown in Fig. 6. With the increase of MB concertation in solution, the adsorption capacity of all samples increased at first and then gradually achieved a constant value finally. Only tiny amount of MB (~20 mg/L) was adsorbed by pure SiO_2-24. With the decoration of Ag, adsorption capacity of all the composites increased significantly. Among all the composites, Ag/SiO_2-24 exhibited the highest adsorption capacity with a value of ~55 mg/g, which is more than two times of pure SiO_2. The high adsorption capacity should be contributed by its high Ag loading (Table 2), which provides more adsorption sites for MB [24].

The effect of pH values on the adsorption of MB onto Ag/SiO_2-24 samples was further conducted. The removal efficiency at different pH as a function of adsorption time is shown in Fig. 7 and the corresponding successive UV–Vis spectra can be seen in Fig. S4. With the increase of solution pH from 3 to 11, the removal efficiency of Ag/SiO_2-24 increased gradually. This behavior could be associated with the electrostatic interaction between Ag/SiO_2-24 and MB. According to the results shown in Fig. S5, Ag/SiO_2-24 is negatively charged in the solution with pH value >3, moreover, absolute value of the negative zeta potential of Ag/SiO_2-24 improved with increasing pH value of the solution. Consequently, more electronegative charges were formed on the surface of Ag/SiO_2-24, meanwhile, there were less competition between H^+ and positively charged MB cations during adsorption as the solution PH increased. As a result of this, the adsorption capacity of Ag/SiO_2-24 increased [36, 37].

The recyclability of Ag/SiO_2-24 for MB adsorption was also evaluated. After adsorption, Ag/SiO_2-24 was collected by centrifugation, washed with fresh $NaBH_4$ solution (1.5 mmol/L) and ethanol solution several times. It can be seen from Fig. S6 that the Ag/SiO_2-24 material still maintained high MB removal efficiency with more than 99% of MB removed even after eight cycles of adsorption–desorption.

3.3 Catalytic reduction of MB

The catalytic reduction of MB with an excess amount of $NaBH_4$ was selected as a model reaction to test the catalytic performance of different Ag/SiO_2 samples. The reaction can be easily monitored by the color change of MB solution after addition of composite sample and $NaBH_4$. Figure 8a shows that all the Ag decorated samples exhibit good catalytic reduction activity for MB, with much higher removal efficiency than that of pure SiO_2 sample. Among those silver containing samples, Ag/SiO_2-24 shows the fastest reduction kinetics, i.e. a completed catalytic reduction of MB within 3 mins (Fig. 9b, c) and removal efficiency > 99%. Comparatively, the time used for complete catalytic reduction using Ag/SiO_2-6, Ag/SiO_2-12, and Ag/SiO_2-48 were 18, 13, and 7 min under the same conditions (Fig. 8a and S7). The catalytic activity based on the Ag content was calculated and listed in Table 3. It could be seen that the higher content of silver, the faster reaction rate was obtained

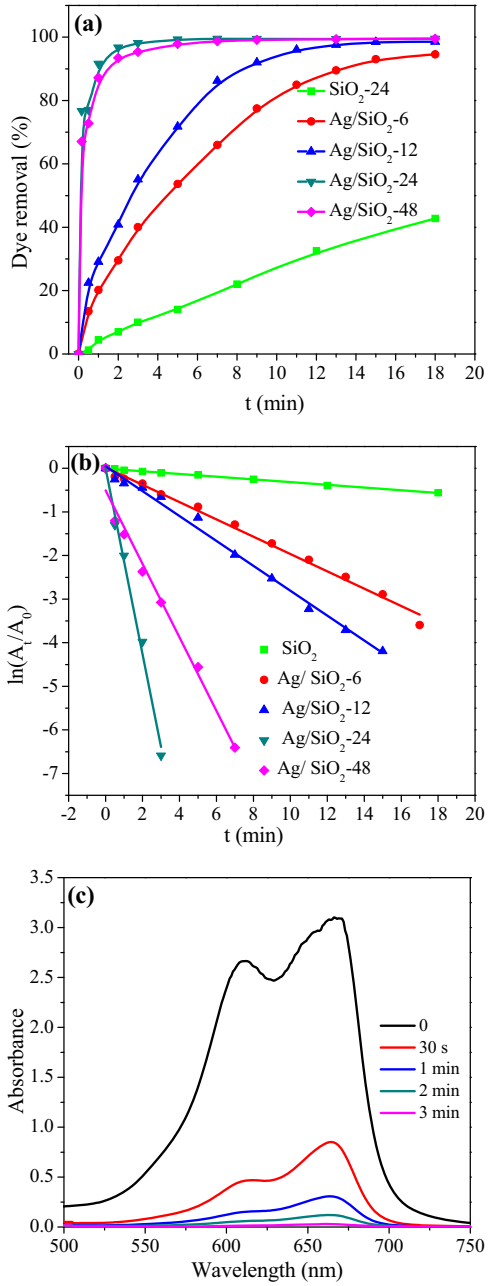

Fig. 8 **a** Fraction of dye degradation during the catalytic reduction of MB. **b** First-order kinetic plot of catalytic MB reduction in the presence of SiO_2-24 and various Ag/SiO_2 samples. **c** Successive UV–Vis spectra for MB reduction with Ag/SiO_2-24 sample. (MB = 40 mg/L, $NaBH_4$ = 0.1 mol/L, solution volume = 20 mL, sample mass = 10 mg, T = 25 °C)

over the corresponding sample, since the silver nanoparticles act as the catalytic sites in the reaction, consequently more active sites were present on the sample with higher Ag content (the particle size of Ag on those samples are very close).

For further analyze the reaction mechanism, pseudo-first-order kinetics model was attempted for simulation for the

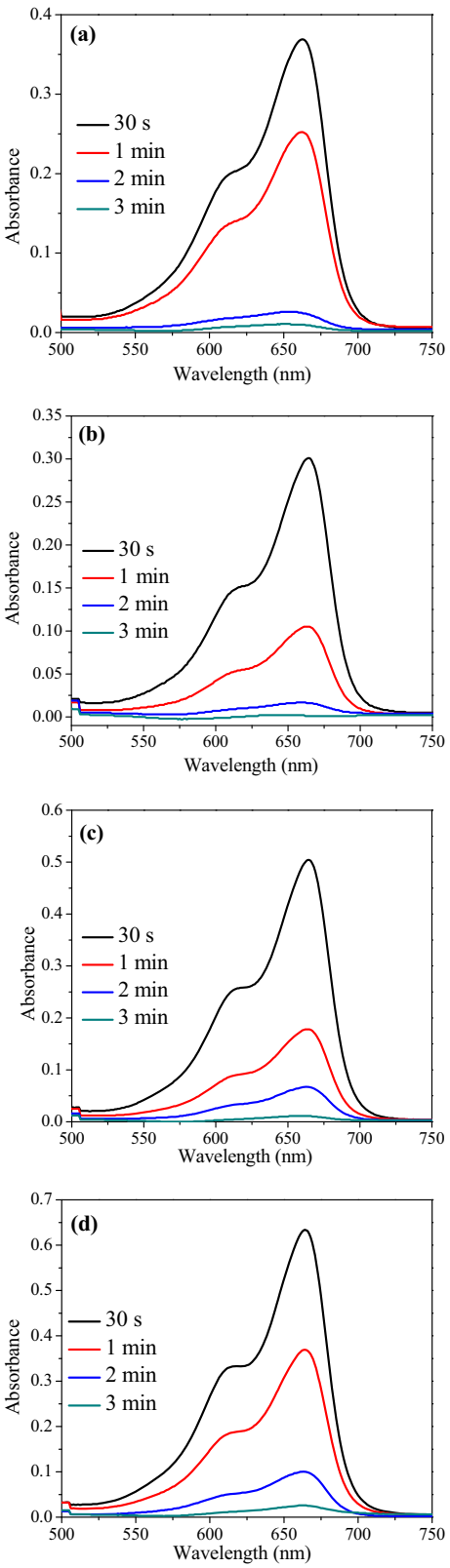

Fig. 9 Successive UV–Vis spectra for catalytic reduction of MB by $NaBH_4$ and Ag/SiO_2-24 sample at **a** pH 3, **b** pH 7, **c** pH 9, and **d** pH 11. (MB = 40 mg/L, $NaBH_4$ = 0.1 mol/L, solution volume = 20 mL, Ag/SiO_2-24 = 10 mg, T = 25 °C)

Table 3 Comparison of rate constants for degradation of MB with different silver composites

Samples	MB/$NaBH_4$ (mol/mol)	Catalyst (g/L)	Ag content (g/L)	Rate constant (k_{app}/ min^{-1})	R^2	References
Ag/Tr-SBA-15	1/40	0.5	–	0.858	–	[21]
Ag/AMT-SBA-15	1/40	0.5	–	0.564	–	[21]
Fe_3O_4@PDA-Ag	1/40	0.5	–	0. 430	0.987	[24]
Ag/SiO_2-6	1/40	0.5	0.018	0.199	0.993	This work
Ag/SiO_2-12	1/40	0.5	0.025	0.285	0.993	This work
Ag/SiO_2-24	1/40	0.5	0.034	2.128	0.990	This work
Ag/SiO_2-48	1/40	0.5	0.030	0.843	0.982	This work
SiO_2-24	1/40	0.5	0	0.032	0.995	This work

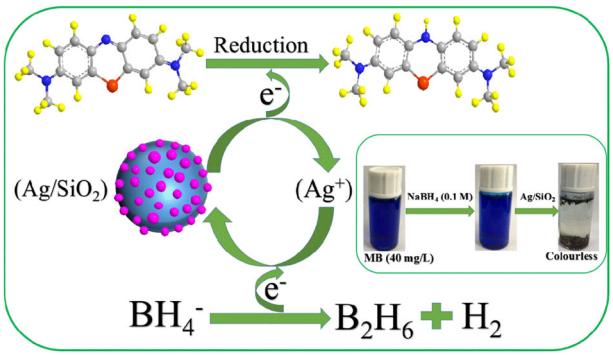

Fig. 10 Mechanism of the catalytic reduction of MB by $NaBH_4$ and Ag/SiO_2 samples

constant concentration and excessive amount of $NaBH_4$ presented. A linear relationship could be observed between $\ln(A_t/A_0)$ vs. time plots for all samples in Fig. 8b. The rate constants of MB catalytic reduction were calculated to be 0.199, 0.285, 2.128, and 0.842 min^{-1} at 25 °C for Ag/SiO_2-6, Ag/SiO_2-12, Ag/SiO_2-24, and Ag/SiO_2-48 samples, respectively (Table 3). Obviously, k_{app} value of Ag/SiO_2-24 was much higher than other samples, possibly owing to a higher Ag content in Ag/SiO_2-24. Moreover, a comparison of the values (Table 3) reveals that Ag/SiO_2-24 shows significant higher k_{app} value compared with the catalyst reported in literature. Thus, Ag/SiO_2-24 sample was selected for further analysis because of its superior catalytic activity.

To explore the effect of solution pH on catalytic degradation of MB with Ag/SiO_2-24 sample, MB solutions with four different pH values (pH = 3, 7, 9, 11) were prepared for the study. It could be clearly seen (Fig. 9) that there is little change in catalytic activity of Ag/SiO_2-24 in the solution with pH range of 3–11, with removal efficiency for MB up to > 99% within 3 min, indicating that Ag/SiO_2-24 can maintain high catalytic activity in a wide range of solution pHs.

The electron transfer effect can be used to explain the catalytic reduction of dye by Ag/SiO_2 composites [38–41]. Silver is a good conductor and can transfer electrons between donors and receptors. Therefore, this catalytic process can be mediated by silver nanoparticles through redox mechanism, and electrons can be transferred from donor (BH_4^-) to the acceptor (MB) [24, 42]. Figure 10 displays the illustration of general reduction of MB in the presence of Ag/SiO_2 and $NaBH_4$. Firstly, $NaBH_4$ and MB were adsorbed onto the surface of Ag/SiO_2. Then, electrons can be transferred from BH_4^- to MB with the help of Ag catalyst, resulting in the reduction of MB into LMB (leucomethyene blue) (Fig S8). Finally, LMB spontaneously desorbed from the surface of Ag/SiO_2 and diffused into the solution due to weaker electrostatic action between Ag/SiO_2 and LMB [33, 38].

3.4 Catalyst stability

The recyclability of catalytic materials is an important standard for practical application. Figure 11a shows that the Ag/SiO_2-24 sample displays good recycle performance with extremely high removal efficiency for MB even after four cycles of catalytic reduction. Moreover, there is little change in XRD diffraction patterns before and after reaction (Fig. 11b), demonstrating that structure of the materials was well reserved after catalytic runs. FT-IR spectra were collected to further explore the surface functional groups of Ag/SiO_2-24 before and after reaction (Fig. 11c). The peaks at 800 cm^{-1} (Si-O-Si), 959 cm^{-1} (Si-OH), and 1098 cm^{-1} (Si-O-Si) remained unchanged, indicating the stable surface functional groups of the materials.

This study also evaluated the stability of Ag/SiO_2 in strong acidic environment. After 24 h of continuous stirring of 10 mg of Ag/SiO_2-24 dispersed in 20 ml of deionized water with pH values of 2 or 3, the concentrations of silver ion in the solution were measured by inductively coupled plasma mass spectrometry (ICP-MS, Agilent 7900). The data shown in Table 4 revealed that only about 1.3% and 0.6% of silver in Ag/SiO_2-24 composite was leached out in the environment of pH = 2 and pH = 3, respectively. This result suggested that Ag/SiO_2 can possibly be applied in strong acidic environment owing to its high stability.

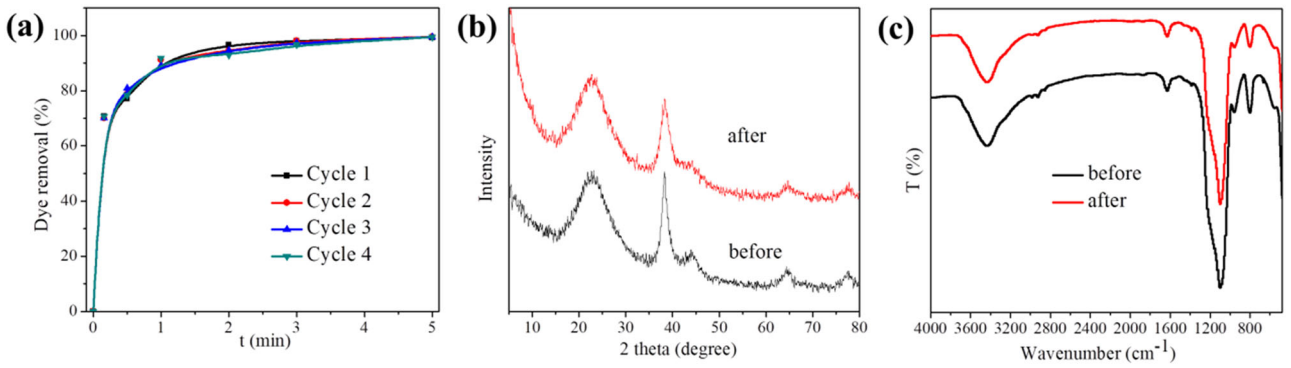

Fig. 11 **a** Recyclability of Ag/SiO_2-24 sample during the catalytic reduction of MB with $NaBH_4$ (MB = 40 mg/L, $NaBH_4$ = 0.1 M, sample = 0.5 g/L, T = 25 °C), **b** XRD patterns, and **c** FT-IR spectra of Ag/SiO_2-24 before and after catalytic reduction of MB

Table 4 Silver precipitation of Ag/SiO_2-24 composite under acid conditions

Sample	pH	C_{Ag+} (mg/L)	$W_{Ag+}/W_{Ag\ in\ sample}$ (%)
Ag/SiO_2-24	2	0.44	1.3
Ag/SiO_2-24	3	0.21	0.6

4 Conclusions

In summary, highly dispersed silver nanoparticles on rough surface of silica spheres were prepared through simple sol-gel and wet-impregnation methods. These Ag decorated silica shows good adsorption and catalytic capability for MB removal. Among these composites, Ag/SiO_2-24 nanoparticles showed highest MB adsorption capacity of ~55 mg/g and catalytic activity for the reduction of MB with an excess of $NaBH_4$. MB could be catalytically degraded to <1% of the initial concentration within 3 min and the rate constant could be as high as 2.128 min^{-1}. The Ag/SiO_2-24 nanoparticle can also be used in environment with wild range of pH values. Moreover, the as-prepared Ag/SiO_2-24 exhibited excellent reusability for at least 8 cycles of adsorption and 4 cycles of catalytic reduction.

Acknowledgements This work was supported by the Fundamental Research Funds for the Central Universities (No. 2018XKQYMS18) and the Priority Academic Program Development of Jiangsu Higher Education Institutions.

Compliance with ethical standards

Conflict of interest The authors declare that they have no conflict of interest.

References

1. Bruggen BVD, Vandecasteele C, Gestel TV, Doyen W, Leyse R (2003) A review of pressure-driven membrane processes in wastewater treatment and drinking water production Environ Prog Sustain 22:46–56
2. Bhatnagar A, Sillanpää M (2010) Utilization of agro-industrial and municipal waste materials as potential adsorbents for water treatment—A review. Chem Eng J 157:277–296
3. Zhou J, Tang C, Cheng B, Yu J, Jaroniec M (2012) Rattle-type carbon–alumina core–shell spheres: synthesis and application for adsorption of organic dyes. Mater ACS Appl Interfaces 4:2174–2179
4. Hu M, Yan X, Hu X, Zhang J, Feng R, Zhou M (2018) Ultra-high adsorption capacity of MgO/SiO_2 composites with rough surfaces for Congo red removal from water. J Colloid Interf Sci 510:111–117
5. Rodríguez A, Ovejero G, Sotelo JL, Mestanza M, García J (2010) Heterogeneous Fenton catalyst supports screening for mono azo dye degradation in contaminated wastewaters. Ind Eng Chem Res 49:498–505
6. Fathima NN, Aravindhan R, RaghavaRao J (2008) Dye house wastewater treatment through advanced oxidation process using Cu-exchanged Y zeolite: A heterogeneous catalytic approach. Chemosphere 70:1146–1151
7. Feng J, Hu X, Yue PL (2004) Discoloration and mineralization of orange II using different heterogeneous catalysts containing Fe: A comparative study. Environ Sci Technol 38:5773–5778
8. Pan C, Zhu Y (2010) New type of BiPO4 oxy-acid salt photocatalyst with high photocatalytic activity on degradation of dye. Environ Sci Technol 44:5570–5574
9. Subash B, Krishnakumar B, Swaminathan M, Shanthi M (2013) Highly efficient, solar active, and reusable photocatalyst: Zr-loaded Ag–ZnO for reactive red 120 dye degradation with synergistic effect and dye-sensitized mechanism. Langmuir 29:939–949
10. Qiu W, Yang H, Wan L, Xu Z (2015) Co-deposition of catechol/polyethyleneimine on porous membranes for efficient decolorization of dye water. J Mater Chem A 3:14438–14444
11. Brillas E, Martínez-Huitle CA (2015) Decontamination of wastewaters containing synthetic organic dyes by electrochemical methods, An updated review. Appl Catal B-Environ 166-167:603–643
12. Hayat H, Mahmood Q, Pervez A, Bhatti ZA, Baig SA (2015) Comparative decolorization of dyes in textile wastewater using biological and chemical treatment. Sep Purif Techol 154:149–153
13. Matatov-Meytal YI, Sheintuch M (1998) Catalytic abatement of water pollutants. Ind Eng Chem Res 37:309–326
14. Gupta VK, Carrott PJM, Ribeiro Carrott MML (2009) Suhas, low-cost adsorbents: Growing approach to wastewater treatment-a review. Crit Rev Env Sci Tec 39:783–842

15. Zhang J, Yan X, Hu X, Feng R, Zhou M (2018) Direct carbonization of Zn/Co zeolitic imidazolate frameworks for efficient adsorption of Rhodamine B. Chem Eng J 347:640–647
16. Song Z, Chen L, Hu J, Richards R (2009) NiO(111) nanosheets as efficient and recyclable adsorbents for dye pollutant removal from wastewater. Nanotechnology 20:275707
17. Cheng Z, Liao J, He B, Zhang F, Huang X, Zhou L (2015) One-step fabrication of graphene oxide enhanced magnetic composite gel for highly efficient dye adsorption and catalysis. ACS Sustain Chem Eng 3:1677–1685
18. Darmograi G, Prelot B, Layrac G, Tichit D, Martin-Gassin G, Salles F, Zajac J (2015) Study of adsorption and intercalation of orange-type dyes into Mg-Al layered double hydroxide. J Phys Chem C 119:23388–23397
19. Pradhan AC, Parida KM (2012) Facile synthesis of mesoporous composite Fe/Al_2O_3–MCM-41: an efficient adsorbent/catalyst for swift removal of methylene blue and mixed dyes. J Mater, Chem 22:7567–7579
20. Abbas M, Torati SR, Kim CG (2015) A novel approach for the synthesis of ultrathin silica-coated iron oxide nanocubes decorated with silver nanodots (Fe_3O_4/Ag/SiO_2) and their superior catalytic reduction of 4-nitroaniline. Nanoscale 7:12192–12204
21. Saad A, Snoussi Y, Abderrabba M, Chehimi MM (2016) Ligand-modified mesoporous silica SBA-15/silver hybrids for the catalyzed reduction of methylene blue. RSC Adv 6:57672–57682
22. Ghosh S, Vandana V (2017) Nano-structured mesoporous silver/silica composite: Synthesis, characterization and targeted application towards water purification. Mater Res Bull 88:291–300
23. Shen H, Duan C, Guo J, Zhao N, Xu J (2015) Facile in situ synthesis of silver nanoparticles on boron nitride nanosheets with enhanced catalytic performance. J Mater Chem A 3:16663–16669
24. Xie Y, Yan B, Xu H, Chen J, Liu Q, Deng Y, Zeng H (2014) Highly regenerable mussel-inspired Fe3O4@Polydopamine-Ag core–shell microspheres as catalyst and adsorbent for methylene blue removal. ACS Appl Mater Interfaces 6:8845–8852
25. Wang F, Li F, Xu M, Yu H, Zhang J, Xia H, Lang J (2015) Facile synthesis of a Ag(I)-doped coordination polymer with enhanced catalytic performance in the photodegradation of azo dyes in water. J Mater Chem A 3:5908–5916
26. Kang H, Zhu Y, Yang X, Jing Y, Lengalova A, Li C (2010) A novel catalyst based on electrospun silver-doped silica fibers with ribbon morphology. J Colloid Interf Sci 341:303–310
27. Dubey SP, Dwivedi AD, Kim I, Sillanpaa M, Kwon Y, Lee C (2014) Synthesis of graphene-carbon sphere hybrid aerogel with silver nanoparticles and its catalytic and adsorption applications. Chem Eng J 244:160–167
28. Rostami-Vartooni A, Nasrollahzadeh M, Alizadeh M (2016) Green synthesis of seashell supported silver nanoparticles using Bunium persicum seeds extract: Application of the particles for catalytic reduction of organic dyes. J Colloid Interf Sci 470:268–275
29. Rostami-Vartooni A, Nasrollahzadeh M, Alizadeh M (2016) Green synthesis of perlite supported silver nanoparticles using Hamamelis virginiana leaf extract and investigation of its catalytic activity for the reduction of 4-nitrophenol and Congo red. J Alloy Compd 680:309–314
30. Wang W, Wang P, Tang X, Elzatahry AA, Wang S, Al-Dahyan D, Zhao M, Yao C, Hung C, Zhu X, Zhao T, Li X, Zhang F, Zhao D (2017) Facile synthesis of uniform virus-like mesoporous silica nanoparticles for enhanced cellular internalization. ACS Cent Sci 3:839–846
31. Xu Z, Yu J, Liu G, Cheng B, Zhou P, Li X (2013) Microemulsion-assisted synthesis of hierarchical porous Ni(OH)2/SiO2 composites toward efficient removal of formaldehyde in air. Dalton T 42:10190–10197
32. Abbas M, Torati SR, Kim CG (2015) A novel approach for the synthesis of ultrathin silica-coated iron oxide nanocubes decorated with silver nanodots (Fe_3O_4/SiO_2/Ag) and their superior catalytic reduction of 4-nitroaniline. Nanoscale 7:12192–12204
33. Fan L, Guo R (2008) Growth of dendritic silver crystals in CTAB/SDBS mixed-surfactant solutions. Cryst Growth Des 8:2150–2156
34. Zhang J, Yan X, Hu M, Hu X, Zhou M (2018) Adsorption of Congo red from aqueous solution using ZnO-modified SiO_2 nanospheres with rough surfaces. J Mol Liq 249:772–778
35. Hernández MA, González AI, Corona L, Hernández F, Rojas F, Asomoza M, Solís S, Portillo R, Salgado MA (2009) Chlorobenzene, chloroform, and carbon tetrachloride adsorption on undoped and metal-doped sol–gel substrates (SiO_2, Ag/SiO_2, Cu/SiO_2 and Fe/SiO_2). J Hazard Mater 62:254–263
36. Gupta N, Singh HP, Sharma RK (2011) Metal nanoparticles with high catalytic activity in degradation of methyl orange: An electron relay effect. J Mol Catal A: Chem 335:248–252
37. Impert O, Katafias A, Kita P, Mills A, Pietkiewicz-Graczyk A, Wrzeszcz G (2003) Kinetics and mechanism of a fast leuco-Methylene Blue oxidation by copper(II)–halide species in acidic aqueous media. Dalton Trans 0:348–353
38. Gao H, Sun Y, Zhou J, Xu R, Duan H (2013) Mussel-inspired synthesis of polydopamine-functionalized graphene hydrogel as reusable adsorbents for water purification. ACS Appl Mater Interfaces 5:425–432
39. Mallick K, Witcomb M, Scurrell M (2006) Silver nanoparticle catalysed redox reaction: An electron relay effect. Mater Chem Phys 97:283–287
40. Zheng Y, Wang A (2012) Ag nanoparticle-entrapped hydrogel as promising material for catalytic reduction of organic dyes. J Mater Chem 22:16552–16559
41. Takai A, Kamat PV (2011) Capture, store, and discharge. Shuttling photogenerated electrons across TiO_2-silver interface. ACS Nano 5:7369–7376
42. Rad AS, Mirabi A, Binaian E, Tayebi H (2011) A review on glucose and hydrogen peroxide biosensor based on modified electrode included silver nanoparticles. Int J Electrochem Sci 6:3671–3683